

Article

Bio-Geochemical Processes: Insights from Fe-Mn Mineralization in the Aegean Sea (Greece)

Charalampos Vasilatos ^{*}, Evdokia E. Kampouroglou, Ifigeneia Megremi and Maria Economou-Eliopoulos 

Department of Economic Geology and Geochemistry, Faculty of Geology and Geoenvironment, National and Kapodistrian University of Athens, 15 784 Athens, Greece

^{*} Correspondence: vasilatos@geol.uoa.gr

Abstract: In this study, we have compiled new and existing mineralogical and geochemical data on Fe-Mn mineralization from the Aegean region [Attica (Grammatiko, Legrena, and Varnavas), Evia and Milos islands], aiming to provide new insights on the genesis of Fe-Mn mineralization in that region and its potential environmental implications. A common feature of those deposits is the relatively low Cr, Co, V, Ni, Mo, and Cd content, whereas Ba, As, W, Cu, Pb, and Zn show remarkably variable values. The Mn-Fe deposits from Milos exhibit the highest tungsten content, while a positive trend between MnO and W, combined with a negative trend between MnO and Fe₂O₃ suggests the preference of W to Mn-minerals. The occurrence of bacterio-morphic Fe-Mn-oxides/hydroxides within Mn-Fe mineralizations in the studied region, indicates the important role of micro-organisms into redox reactions. Moreover, the presence of micro-organisms in the Fe-Mn-deposits, reflecting the presence of organic matter confirms a shallow marine environment for their deposition. A salient feature of the Varnavas and Milos Mn-Fe ores is the presence of sodium chloride coated fossilized micro-organisms, suggesting development from a solution containing relatively high Na and Cl concentrations. Furthermore, from an environmental point of view, consideration is given to the bioavailability of elements such as As, Pb, and W, related to the above-mentioned mineralizations. The high bio-accumulation factor for W ($W_{\text{plant}}/W_{\text{soil}} \times 100$) recorded in the Neogene sedimentary basins of Attica, related to the Grammatiko Fe-Mn mineralization, reflects the high W mobility under alkaline conditions and the potential environmental impact of similar deposits with elevated W content.

Keywords: Fe-Mn ores; fossilized micro-organisms; tungsten; Attic-Cycladic crystalline belt; Greece



Citation: Vasilatos, C.; Kampouroglou, E.E.; Megremi, I.; Economou-Eliopoulos, M. Bio-Geochemical Processes: Insights from Fe-Mn Mineralization in the Aegean Sea (Greece). *Minerals* **2022**, *12*, 1303. <https://doi.org/10.3390/min12101303>

Academic Editor: Santanu Banerjee

Received: 12 September 2022

Accepted: 13 October 2022

Published: 16 October 2022

Publisher's Note: MDPI stays neutral with regard to jurisdictional claims in published maps and institutional affiliations.



Copyright: © 2022 by the authors. Licensee MDPI, Basel, Switzerland. This article is an open access article distributed under the terms and conditions of the Creative Commons Attribution (CC BY) license (<https://creativecommons.org/licenses/by/4.0/>).

1. Introduction

Our understanding of iron-oxide and manganese-oxide/hydroxide ore deposits is based on a geological, geochemical, and geophysical database, such as within the Attic-Cycladic metallogenic belt [Attic-Cycladic Massif or Attic-Cycladic crystalline belt (ACCB)], related to both Mesozoic (e.g., Andros and Evia islands) and Pliocene-Pleistocene (Milos and Santorini islands) submarine hydrothermal activity in the South Aegean Volcanic Arc (SAVA) [1–11], (Figure 1). Most of the current Aegean submarine hydrothermal areas on the SAVA are located at relatively shallow depths (less than 200 m water depth) and are characterized by a large volume of gas released, both because of the degassing of the subducted slab and the mantle wedge as well as the thermal and chemical breakdown of the components of the marine sediments [2,3].

The role of micro-organisms in such mineralizations has been discussed by various researchers (e.g., [2,12–14]). Manganese in nature mostly exists in the oxidation state ranging from +2, +3, and +4 [15]. The existence of Mn oxidizing micro-organisms have been reported since 1901 [16], and many authors have suggested Mn(II) oxidation as it is an energetically favorable process facilitated by different microbes, which are able to utilize energy out [15,17,18]. Mn bio-recovery from low grade Mn ores is an attractive topic, and

the bioleaching technique for recovery of Mn from lean grade ores is considered to be an economic alternative to existing metallurgical processes that provides greater flexibility [19]. Micro-organisms, especially hyperthermophilic, have been isolated from Mediterranean hydrothermal vents [2]. Specifically, bacteria populations along an environmental gradient at a shallow submarine hydrothermal vent near Milos Island and fossil environmental evidence for anoxygenic photoferrotrophic deposition in shallow marine waters on the Milos Island have been suggested [12,14,20].

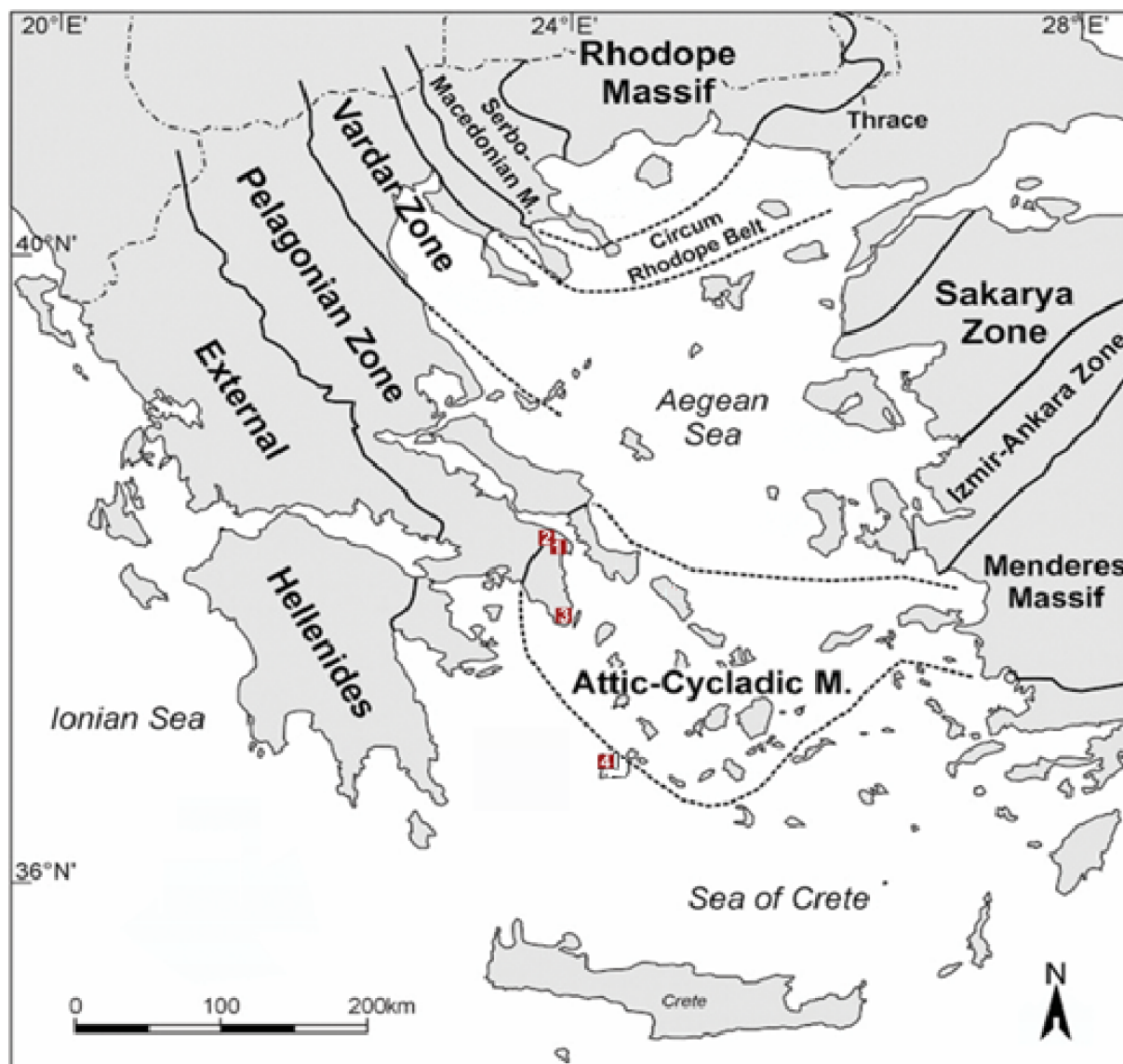


Figure 1. Geological sketch map of Hellenides presenting the main geotectonic units and the locations of the studied Fe-Mn mineralizations in the Attic-Cycladic crystalline belt (Attic-Cycladic M.): 1: Grammatiko, Attica, 2: Varnavas, Attica, 3: Legrena, Attica, 4: Milos island.

The present study focuses on the mineralogical and geochemical characteristics of Fe-Mn mineralization from Milos island, Grammatiko, Legrena and Varnavas Mn-deposit in Attica (e.g., [21,22]). We present new major and trace elements analyses of bulk ore and back scattered electron (BSE) images on unusually thin (a few mm, in thickness) of hard dark brown-black Fe-Mn crusts, revealing the presence of Fe-Mn oxides/hydroxides, forming flakes, tiny spheroid aggregates, micro-nodules or concretions, and fossilized bacteria coated by a NaCl film. Those findings are combined with published geochemical

characteristics, aiming to provide new insights on the genesis of Fe-Mn mineralization and their environmental implications.

2. Geological Outline

The Attic-Cycladic crystalline belt (ACCB) has been described to be composed by three main structural units with different tectono-metamorphic histories (e.g., [23–26]). The Upper Unit (UU) represents the hanging-wall of the Cycladic extensional detachments. It consists of a heterogeneous sequence of Permian to Tertiary sediments, Mesozoic ophiolites and pre-Eocene metamorphic rocks and mélanges with metaigneous blocks and tectonic slabs, transgressively covered by Late Cretaceous unmetamorphosed carbonates, as well as Late Cretaceous medium-pressure/high-temperature rocks and granitoids (e.g., [27–30]).

The structurally intermediate unit is equivalent to the Cycladic Blueschist Unit (CBU) that is the dominant tectonic unit in the Cyclades region. The “allochthonous” CBU consists of remnants of pre-Alpine crystalline basement rocks and a stack of tectonic subunits comprised of a metamorphosed volcano–sedimentary succession [29]. The CBU has undergone regional eclogite- and blueschist-facies metamorphism during Late Cretaceous to Eocene compression (M1 metamorphic event) [29,31]. The Blueschist facies event was followed by a late Oligocene–Miocene, mostly greenschist-facies overprint (M2) with peak conditions of ~450–500 °C and 4–9 kbar [25,28]. In the CBU, there are widespread tectonic slices of ultramafic rocks, intercalated with marbles, metapelites, mafic volcanites and flysch [30]. These exposures include the metamorphic rocks in Andros and in other Cycladic islands and, further north, the Styra-Ochi unit of southern Evia [32], the Lavrion Blueschist Unit [33], and the Hymittos Mountain, Attica [34]. Specifically, the eastern and southern parts of Attica, where the metamorphic section of the ACCB occurs, have been metamorphosed under high pressure and low temperature conditions [35–38]. The UU (equals to Pelagonian geo-tectonic zone) is separated from the CBU by the Attica detachment fault that starts from the eastern Evia in the east and extends into the Saronic Gulf in the west [39].

The structurally lower unit of the ACCB, the para-autochthonous Basal unit, mainly consists of a thick series of Mesozoic marbles and schists with minor lenses of mafic and ultramafic rocks, overlain by a metapelitic sequence. Mineralogical data suggest that the Basal unit has undergone a pre- or early Miocene HP-metamorphism. The area of Lavrion in south Attica constitutes the westernmost part of the ACCB where the allochthonous CBU overthrusts the para-autochthonous Basal unit. The tectonic contact of these units forms a crustal scale thrust zone which is the continuation of the Evia thrust.

In general, mineralization in the ACCB is associated with successive stages of tectono-magmatic evolution and is closely related to extensional faulting [40]. Those magmatic-hydrothermal deposits within ACCB have been investigated extensively by [1,3,41–46]. The widespread carbonate-hosted massive sulfide Pb–Zn–Ag mineralization in Lavrion (south Attica) is spatially related to the detachment fault, shear bands within marbles, and the contact between marbles and the intercalated metaclastics. Ascending hydrothermal fluids deposited massive sulfide ore in carbonate rocks, while skarn-type mineralization is associated with contact metamorphism and subsequent fluid infiltration around granitoid intrusions [41–43]. The presence of the three depositional basins at the Vani area, Milos, has been well established by the sequence of lithologies in each fault-bound unit of varying thickness, which are not present within all the basins and have been interpreted as a result of local syntectonic sediment formation, redox conditions, and/or post-depositional erosion [20,47,48].

The Fe-Mn mineralization in ACCB (Grammatiko, Varnavas, Legrena and Hymittos in Attica and Milos islands (Figure 1) represents a multistage remobilization and redeposition of metals, during metamorphism, hydrothermal activity, and weathering of the whole region. The iron-manganese mineralization in the Legrena (W. Lavrion) and Grammatiko areas (Figure 1) is commonly hosted within carbonate rocks, close to the surface on the detachment fault and the contacts between lower and upper marbles with the Kessariani schist [49,50]. A typical iron-rich gossan formation, located at and close to the surface on the

detachment fault, such as at the areas of Elafos and Thorikos (Lavrion), has been interpreted to be formed during supergene processes by downward-penetrating water, oxidation of hypogene sulfide mineralization, and mobilization of metals and re-precipitation, resulted by the interaction of acidic water with marble [50]. Although any continuity between the Grammatiko and the famous ancient massive sulfide Pb–Zn–Ag mines of Lavrion is not obvious, underground mining at Grammatiko has revealed geological and structural relationships between the host rocks and the Fe–Mn deposit that resemble those located at the Lavrion mines [49,51].

The geology and Fe–Mn mineralization located on NW Milos island (Vani area) has been described in detail by [4,7–11,52–56]. Two types of Mn-deposits in Vani have been described: (a) a stratabound hydrothermal deposit of relatively high temperature that formed by penetration of hydrothermal fluids through faults and fissures within a volcanoclastic sandstone and (b) bedded hydrothermal deposits formed during a subsequent stage by fluids migrated along bedding planes of the volcanoclastic sandstone (e.g., [8,10,11,55]).

3. Materials and Methods

Representative samples of massive Fe–Mn ore and of hard dark brown-black Fe–Mn crust were collected from Grammatiko, Varnavas and Legrena valley (Attica), and Milos islands, ACCB (Figure 1). Samples were collected during fieldwork from a depth of some centimeters from each outcrop. After crushing, only the inner parts of each sample were collected for our study.

Polished sections of all samples were examined under a reflected light microscope and a scanning electron microscope (SEM), equipped with Energy Dispersive Spectroscopy (EDS) for elemental micro-analyses. The SEM-EDS analyses were carried out at the Department of Geology and Geoenvironment, University of Athens (NKUA), using a JEOL JSM 5600 scanning electron microscope, equipped with an ISIS 300 OXFORD automated energy dispersive analysis system. Analytical conditions were 20 kV accelerating voltage, 0.5 nA beam current, 2 μ m beam diameter and 50 s count times. The following X-ray lines were used: AsLa, FeKa, NiKa, CoKa, CuKa, CrKa, AlKa, TiKa, CaKa, SiKa, MnKa, MgKa, and ClKa. Pure metals standards were used for Cu, Ni, Co, and Cr and pyrite was used for S and Fe. Standard indium arsenide and 300 s counting time were used for As and the presence of arsenic was confirmed by the X-ray spectrum. In addition to the well-polished, a few polished sections showing unpolished parts and revealing the presence of goethite micro-textures resembling bacterial cell have been gold plated and analyzed under SEM-EDS in order to identify any traces of carbon and other components of organic material.

Major and trace elements in bulk samples were determined by ICP-MS analysis at ACME Laboratories Ltd., Canada. The samples were dissolved using a strong multi-acid (HNO₃–HClO₄–HF) digestion and the residues dissolved in concentrated HCl.

4. Results

4.1. Mineralogical Characteristics of Fe–Mn Mineralization

4.1.1. Iron–Manganese Mineralization at Grammatiko

At the Grammatiko area, Attica, (Figure 2), Fe–Mn mineralization is hosted within brecciated and foliation zones of carbonate rocks, ranging in thinness from a few millimeters to a few meters. The presence of unusually small (a few mm to cm, in thickness) hard dark brown-black Fe–Mn crusts, within the carbonate rocks (Figure 3a,b) is a common feature with those of the Legrena area (W. Lavrion, Attica), alongside their contact with the Kessariani schist. The most abundant minerals in the Fe–Mn ore from the Grammatiko mine are hematite, goethite, and pyrolusite. Veins of calcite cross-cutting the ore are common (Figure 3a). Hematite often contains traces of Mn, Zn, Cu, and S (Table 1). Iron–Mn oxides/hydroxides, with varying Fe/Mn ratio, form flakes, tiny spheroid aggregates, micro-nodules, or concretions.

Table 1. Representative SEM-EDS analyses from Fe-Mn mineralization in Attica and Milos Island.

wt%	Grammatiko						Milos				
	Gsf1 Coronadite	GSf10	Gsf 1d Hematite	Gsf2	Gsf4c Malachite	Gsf5	Mil3 Hollandite	Mil4 Barite	Mil5 Pyrolusite		
SiO ₂	n.d	n.d	n.d	n.d	n.d	n.d	n.d	0.1	n.d		
Fe ₂ O ₃	1.16	1.7	96.6	98.7	n.d	n.d	12.1	0.2	4.1		
Al ₂ O ₃	0.5	0.7	0.2	0.3	0.5	n.d	n.d	n.d	n.d		
MnO	59.8	56.9	n.d	n.d	n.d	n.d	58.4	1.7	89.3		
BaO	1.2	n.d	n.d	n.d	n.d	n.d	14.1	63.1	4.4		
MgO	0.4	n.d	n.d	n.d	n.d	n.d	n.d	0.3	n.d		
CaO	0.6	n.d	n.d	n.d	n.d	n.d	n.d	n.d	n.d		
ZnO	n.d	n.d	n.d	n.d	n.d	n.d	4.5	n.d	1.6		
PbO	27.4	31.8	n.d	n.d	n.d	n.d	n.d	n.d	n.d		
CuO	1.1	1.9	1.5	n.d	69.9	69.3	n.d	n.d	n.d		
As ₂ O ₃	n.d	1.4	n.d	n.d	2.3	n.d	n.d	n.d	n.d		
K ₂ O	n.d	n.d	n.d	n.d	n.d	0.7	n.d	n.d	n.d		
SO ₃	n.d	n.d	n.d	n.d	n.d	n.d	n.d	32.4	n.d		
WO ₃	n.d	n.d	n.d	n.d	n.d	n.d	1.6	3.1	1.4		
P ₂ O ₅	n.d	0.3	n.d	n.d	n.d	n.d	n.d	n.d	n.d		
Cont	92.16	94.7	98.3	99.0	72.7	67.3	90.7	100.9	100.8		
Varnavas											
wt%	Mn-nt	Mn-nt	Mn-nt	Mn-nt	matrix mixed	matrix Epidote	matrix Epidote	matrix Pyroxene	matrix Pyroxene	K-Feldspar	Mg-Calcite
SiO ₂	6.9	3.5	0.9	2.2	40.9	31.7	32.6	34.6	37.2	63.8	n.d
Fe ₂ O ₃	76.2	82.1	90.1	84.8	1.3	17.3	18.2	8.2	8.8	0.5	n.d
Al ₂ O ₃	4.3	2.1	n.d	1.4	4.7	15.5	14.5	1.6	0.9	18.1	n.d
MnO	5.6	6.4	5.9	5.9	n.d	2.7	2.1	1.1	1.8	2.2	n.d
MgO	0.8	1.4	n.d	1.7	n.d	n.d	n.d	1.8	1.2	1.1	8.7
CaO	5.5	3.6	1.3	2.7	27.6	24.3	19.1	41.7	50.1	n.d	44.8
As ₂ O ₃	1.2	n.d	n.d	n.d	20.1	n.d	1.3	n.d	0.8	n.d	n.d
K ₂ O	0.6	0.3	n.d	n.d	n.d	5.2	9.5	0.5	0.4	14.5	n.d
Total	101.1	99.4	98.2	98.7	94.6	96.7	97.3	89.5	101.2	100.2	53.5
Cont											
Milos											
Si	n.d	n.d	n.d	0.9	0.6	0.6					
Na	38.9	36.7	39.3	38.2	40.2	40.6					
Cl	58.3	57.7	53.5	59.1	57.4	56.7					
Pb	2.2	1.2	n.d	n.d	n.d	n.d					
Mn	0.6	1.6	2.5	2.6	2.1	2.1					
Fe	n.d	0.5	0.7	0.4	n.d	n.d					
W	n.d	1.2	n.d	n.d	n.d	n.d					
K	n.d	n.d	n.d	0.3	n.d	n.d					
	100.00	98.9	96	101.5	100.3	100.00					

n.d: not detected.

4.1.2. Supergene Mineralization at Grammatiko

At the area of Grammatiko, there have been also identified dominant supergene minerals in small, oxidized sulphide ore (Figure 4a), mainly oxides, hydroxides, sulfates, and carbonates/hydroxycarbonates, such as goethite, coronadite, malachite, and plumbojarosite (Table 1; Figure 4). This supergene mineralization may be analogous to the supergene mineralization of the Lavrion mines (south Attica) where the massive sulfide ore is intensely oxidized as a result of uplift of the ACCB, the development of fractures under extensional conditions, and subsequently weathering [50].

4.1.3. Legrena (Western Lavrion Area)

The dominant Fe-hydroxide mineral at the Legrena valley mineralization is goethite. Calcite as gangue mineral is almost pure, with Mg and Fe in its crystals being insignificant. Iron-Al-Silicates are common as a component in the matrix. A replacement of Fe-oxides/hydroxides (light grey) by dark grey Mn-Fe hydroxides is a common feature

(Figure 5). A peculiar feature of goethite is its spheroidal, bacterio-morphic shape, in an open space filling case (Figure 5c). Representative back scattered images from spherical Fe-Mn porous ore show a consortium of bacteria fossils (white arrows), including abundant sphere or coccus and filaments within a fine-grained matrix. Although the chemical composition of those fossilized bacteria was not determined exactly, due to their very small size, they exhibit a wide chemical composition, comparable to that of Mn-Fe-hydroxides, containing significant amounts of K, Na, P, S, Ca, Mg, As, Ba and Cl (Table 1).

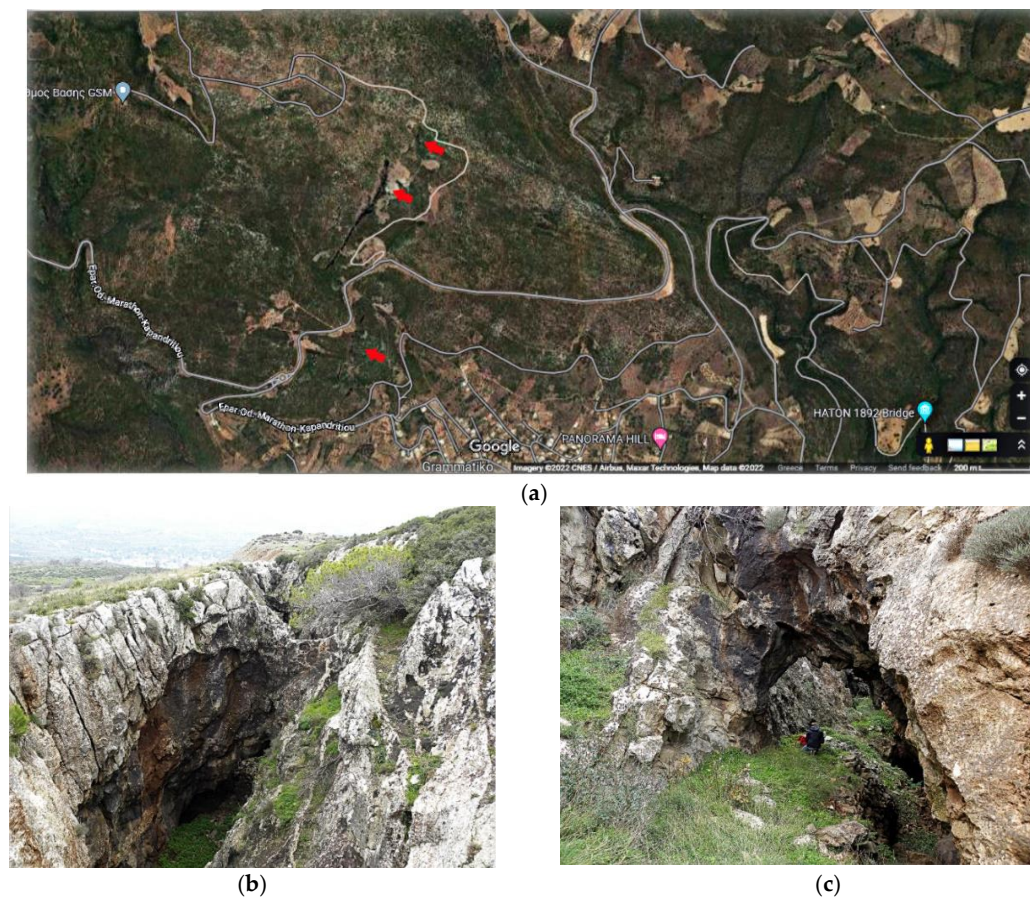


Figure 2. (a) Aerial view of the Grammatiko mines (Google Map) showing the positions of the trenches (red arrows). (b,c) Fe-Mn mineralization is hosted within brecciated and foliation zones of carbonate rocks, ranging in thinness from a few millimeters to a few meters, in ancient mines of Grammatiko (Attica).

Supergene impregnations with Fe-Mn oxides/hydroxides have been observed in hydrothermally altered marbles, presenting a red-brown to yellow-brown color in an abandoned mine located at northern Hymittos Mountain (central Attica), exhibiting a spatial association with unusual silver-rich galena ore (up to 1500 ppm Ag), and As-rich pyrite (up to 3.9 wt% As) in the core of zoned pyrites. This mineralization is hosted in mylonitic marbles that have been affected by brittle-ductile deformation which is associated with the West Cycladic Detachment System [34]. These authors provided isotope data and concluded similarity to the low-temperature carbonate replacement style mineralization in Kamariza, Lavrion mine. Specifically, the isotopically light (-11.2 to -12.2%) values for $\delta^{34}\text{S}$ from galena suggest a sedimentary component to the ore fluid, derived probably from leaching of the meta-sedimentary (calc-mica schists) wall rocks. In addition, the C and O isotopic composition of the carbonate wall rock distal to the orebody is typical of marine carbonates, whereas hydrothermal brown calcite and dolomite are dominated by an external, light C source [34].

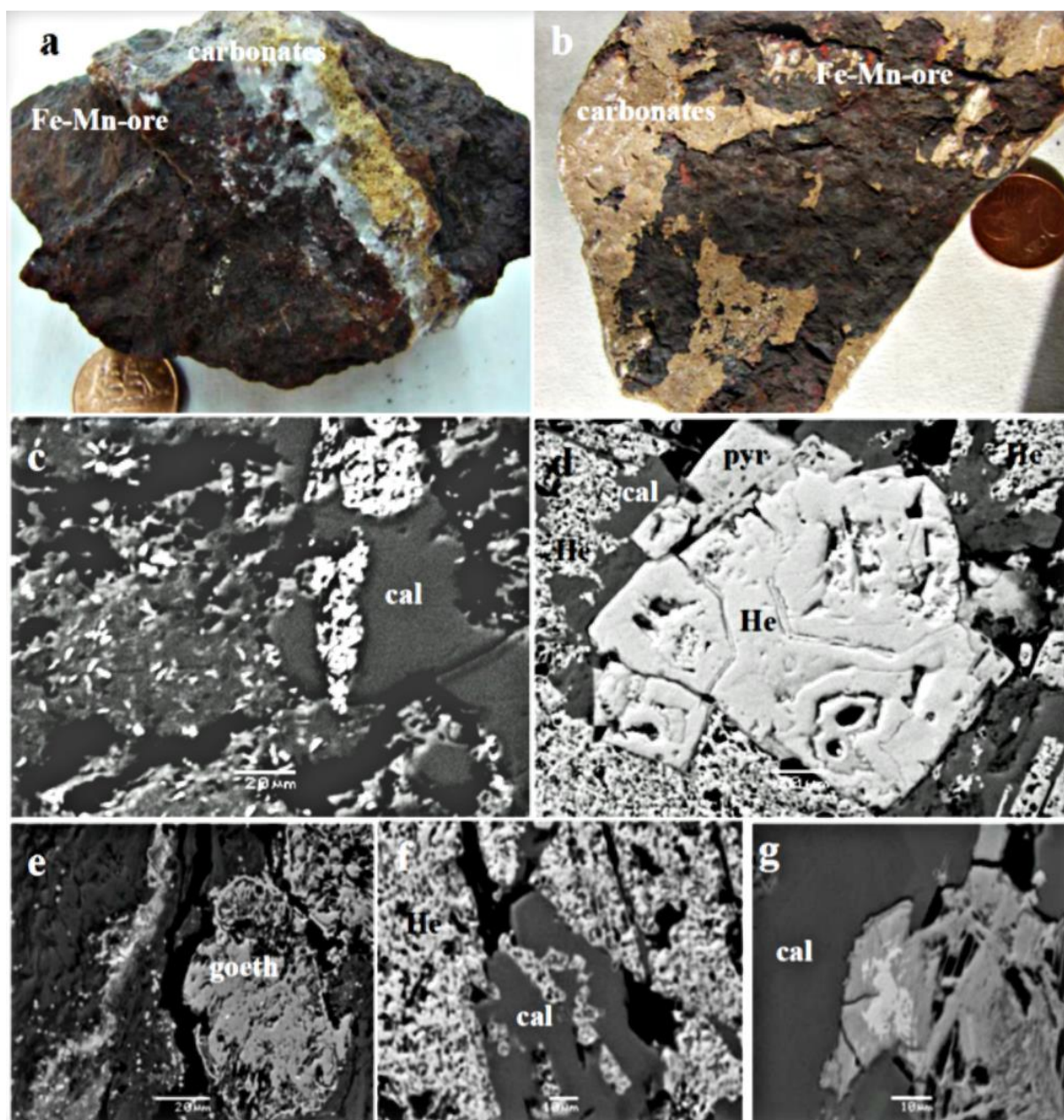


Figure 3. (a) Photograph of massive Fe-Mn ore hosted in limestone, cross-cutting by a carbonate vein, and (b) Fe-Mn mineralization appears as irregular, hard dark brown-black crust, on the carbonate surface. (c–g) Representative back scattered (BSE) images from the Grammatiko mine showing hematite (He, light grey) mostly of fine-grained fossilized bacterio-morphic and large crystals (c,d,f), goethite (goeth) (e), pyrolusite (pyr) (d), and calcite cal (c–g).

4.1.4. Varnavas

Manganese-nodules and Mn-Fe crusts at the Varnavas area, NE Attica (Figure 6), are associated with calcareous schists and quartz-mica schists and have been metamorphosed (greenschist facies) [57]. The dominant minerals in the Mn-Fe ore, which often fill open spaces, are fine-grained Mn-oxide (pyrolusite Mn-rich nodules of Mn-magnetite and hematite in a matrix, mainly consisting of Mn-bearing garnet (grossular-andradite), diopside, epidote, chlorite, K-Feldspar, Mg-calcite, and quartz. A significant feature is the presence of fossilized bacterio-morphic Mn-Fe oxides/hydroxides (Figure 6c,d) coated by a film composed of Na and Cl in a ratio close to that of sodium chloride (NaCl) (Table 1).

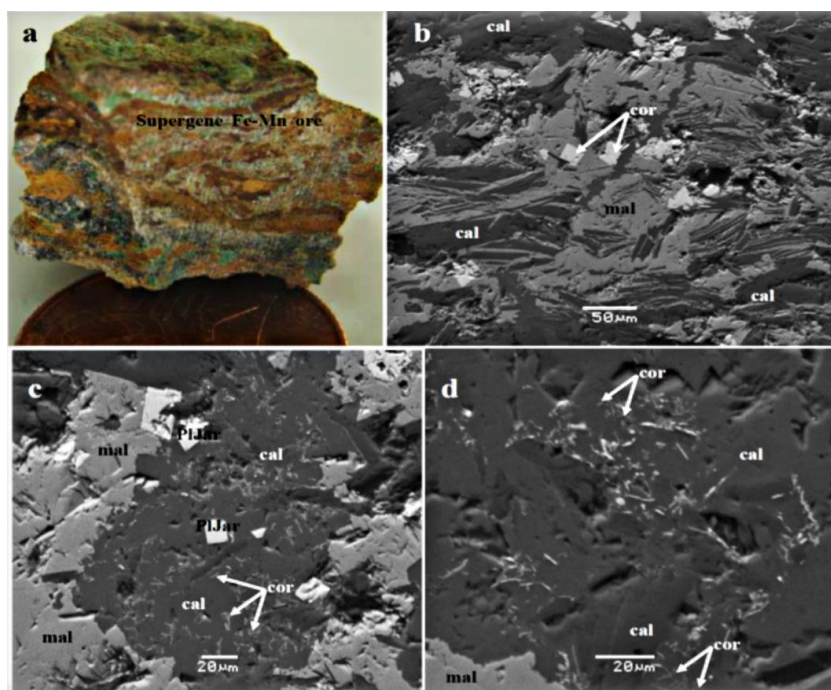


Figure 4. (a) Photograph of the supergene Fe-Mn ore hosted in limestone from the Grammatiko mine. (b–d) Representative back scattered images showing the dominant association of calcite (cal) with coronatite (cor), malachite (mal), and plumbojarosite (PlJar).

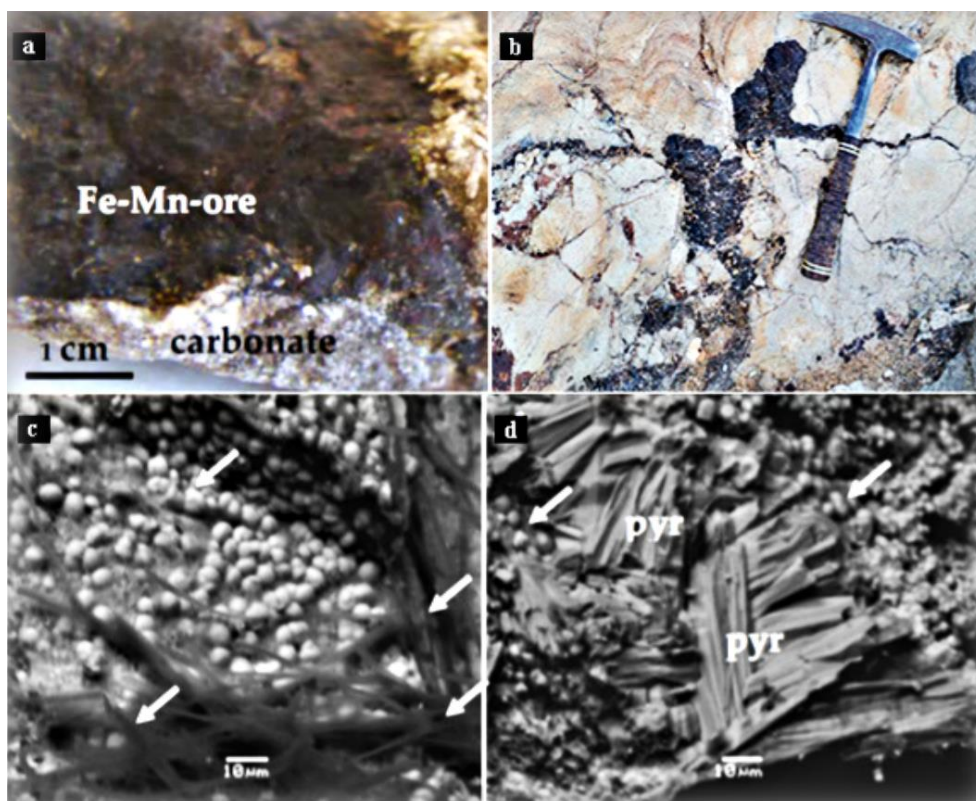


Figure 5. (a,b) Photograph of Fe-Mn ore sample hosted in limestone, from the Legrena area, W. Lavrion, Attica. Scanning electron microscope images showing (c,d): Consortium of bacteria fossils (white arrows) including abundant sphere or coccus (monococcus, diplococcus, or packets) and filaments within a matrix of goethite. Goethite coated spherical fossilized bacteria and fibrous crystals of pyrolusite (pyr) are remarkable.

4.1.5. Milos

The Mn-Fe ore deposits of Milos Island are associated with a sequence of calc-alkaline volcanic-sedimentary rocks that evolved from Middle-Late Pliocene to Late Pleistocene have been extensively studied by previous authors [4,8–11,58]. The present study focuses on the Vani (Milos Island) manganese deposit which is characterized by the presence of botryoidal surfaces of the ore (Figure 7a). The dominant minerals of the studied samples are hematite, hollandite, barite, and pyrolusite. The most salient feature is the presence of fossilized bacteriomorphic Mn-Fe oxides/hydroxides (Figure 7c,d) coated by a film composed by Na and Cl in a proportion close to that of sodium chloride (NaCl) (Table 1).

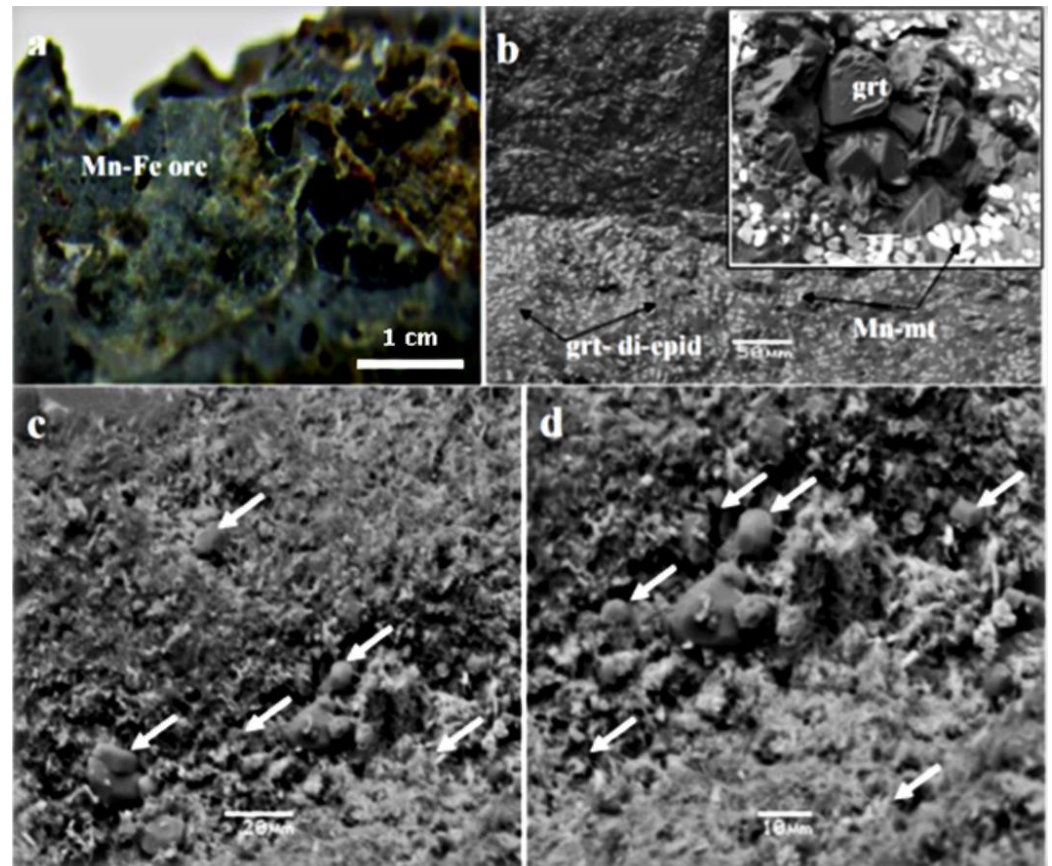


Figure 6. (a) Photograph of massive hydrothermal Mn-Fe ore from the area of Varnavas. (b–d) Back scattered images showing the dominant minerals, Mn-magnetite (Mn-mt) within a matrix consisting mostly of fine-grained Mn-bearing garnet (grt), diopside (di), and epidote (epid) (5b) The presence of fossilized bacterio-morphic Mn-Fe oxides/hydroxides (5c,d); white arrows) coated by a Na and Cl composed film, resembling NaCl (Table 1) is remarkable.

4.2. Geochemical Characteristics

In Table 2, the presented chemical composition of the deposits from Attica (Grammatiko, Legrena of W. Lavion) discriminates them from the Fe-Mn type of ore, whereas those from Evia, Varnavas, and Milos are of Mn-Fe ore type, exhibiting higher Ba content, compared to the former. In general, the Cr, Co, V, Ni, Mo, and Cd content is relatively low, while Ba, As, W, Cu, Pb, and Zn present remarkable variable content (Table 1). The “high temperature” Mn-ores exhibit relatively high Mn, Ba, and Pb values, while the bedded-type show elevated Al, Fe, Ti, Zn, K, Na, Ca, Mg, and Th values (Table 2), [11]. The Mn-Fe ore samples from Milos presented the highest tungsten (W) content (Table 2) which is in good agreement with published geochemical data [10], but any relation to the other elements is not clear.

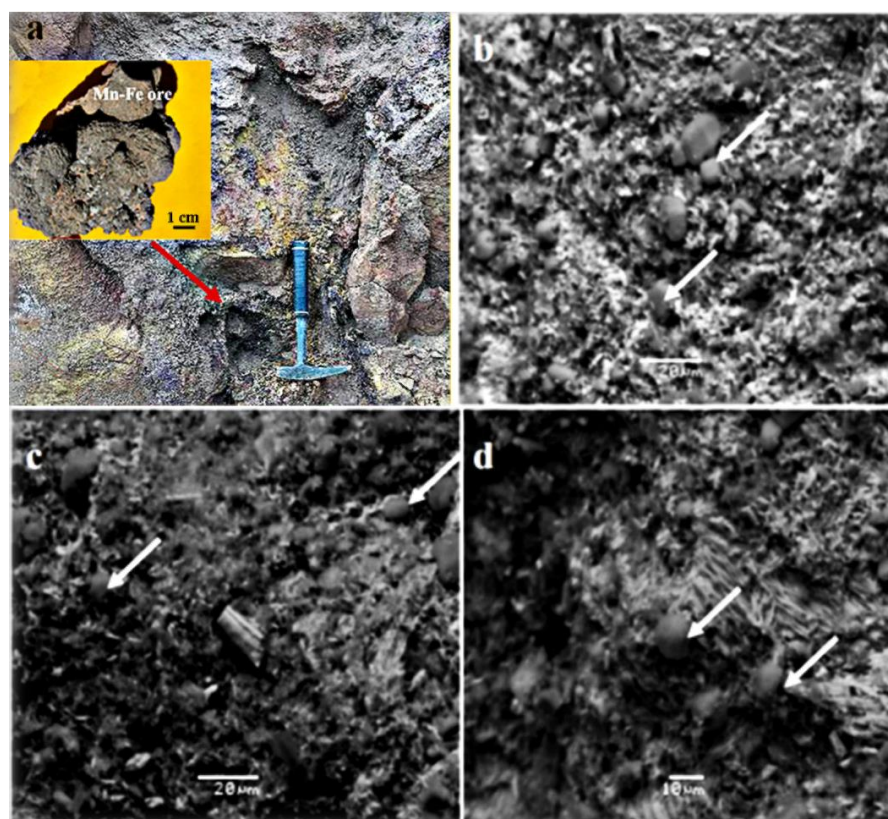


Figure 7. (a) Photograph of botryoidal Mn-Fe ore sample from Vani area, Milos Island. Back scattered scanning electron microscope images showing (b–d): bacteria fossils (white arrows) including abundant sphere or coccus within a matrix of hollandite, pyrolusite, hematite, and barite (see Table 1).

Table 2. Representative bulk analyses of iron-manganese mineralizations from the Aegean Sea.

ppm	Grammatiko		Lavrión		Varnavas	S. Evia		Milos			Milos *	D. Limit	
	Figure 2		Figure 3	Figure 4	Figure 5		Figure 6			Mn-Ore n = 25			
	Massive Mn-Ore G108C	G101A	Super-Genie Ore G108A	Fe-Mn Crust LV1	Massive Fe-Mn Ore LV2	Massive Mn-Ore Var.1	Mn-Ore Evia1	Evia2 **	Massive Mn-Ore Mil.V1			Volcanclastic Sandstone Mil.V2	Mil.V3
Mo	20	0.7	14				6	4.5	26	12.0	0.7		0.5
Cu	1600	1.2	>10,000	6.2	19.2	290	710	750	410	7.0	3.5	870	0.5
Ni	12	1.6	2.6	24	140	3.9	48	39	6	6.9	2.2		0.5
Co	15	2.4	0.9	15	15	15	180	90	40	6	22		1.0
Pb	2850	21	7200	55	5.1	1590	30	1170	9200	14	21	9300	0.5
Zn	3300	150	900	102	17	4090	140	110	6800	37	36	3200	5.0
Cr	1	<1	<1	2	1.4	2	30	14	<1	4	7		1.0
Mn	>10,000	>10,000	1650	2750	6500	>10,000	375,000	170,000	360,900	150	55	300,000	5.0
As	900	58	1600	100	13	1170	2	9	1500	60	240	1100	5.0
Sr	120	110	19	110	18	640	690	1140	1140	160	70	1100	5.0
Cd	12	1.6	61	0.4	0.5	4	3	1.5	6.8	<0.5	>0.5		0.5
Sb	1300	15	400	2.2	10	33	30	6	33	4.5	15	260	0.5
V	3	<2	<2	<2	2	36	110	11	35	84	90		10
La	<1	<1	1	5.1	5	35	36	18	36	14	12	22	0.5
Ba	880	36	9	130	27	9900	620	21,600	90,600	320	910		5.0
W	12	8.4	0.2	65	55	70	20	38	110	23	190	580	0.5
Zr	<0.5	<0.5	<0.5	<0.5	<5	<5	11	21	21	110	60	34	0.5
Y				17	20	60	57	21,600	15	8.5	8.1	20	0.5
%													
Fe	26.17	>40.00	5.26	5.8	55	2.21	1.0	1.0	1.58	2.43	5.16	1.7	0.01
Al	<0.01	0.01	0.15	0.02	0.2	0.11	1.0	1.0	1.82	8.15	7.08	3.1	0.01
Ti	<0.001	<0.001	<0.001	<0.001	<.001	0.03	0.07	0.14	0.07	0.12	0.18	0.01	0.001
Mg	0.08	0.1	0.04	3.4	0.04	0.05	0.32	0.44	0.1	0.57	0.03	0.24	0.01
Ca	12.55	5.36	19.7	27.3	0.05	0.16	0.89	0.83	0.29	1.5	0.07	0.2	0.01
P	<0.01	<0.01	0.03	0.02	0.03	0.02	0.2	<0.01	0.02	<0.01	<0.01		0.01
Na	0.02	0.01	0.01	0.01	0.02	0.17	0.1	0.01	0.31	2.36	0.21	1	0.01
K	0.16	<0.01	0.02	0.01	0.2	0.71	0.9	0.15	3.03	1.12	6.41	1.4	0.01
S	<0.05	<0.05	<0.05	0.06	0.05	<0.1	0.09	<0.05	0.13	<0.05	1.46		0.05

Symbols: * = Glasby et al (2005) [10]; ** = Gkikas (2014) [62]

The bivariate statistics (correlation coefficient) of published analytical data for the “High-temperature” and “Bedded” hydrothermal Mn deposits [10,11] have not revealed any significant correlation between the elements.

The most well pronounced positive correlation ($r = >0.9$) is that between MnO and As, in particular that of high-temperature hydrothermal Mn deposits (Figure 8a) for the majority of the samples. Only a few samples present a separate positive correlation as well (Figure 8a). However, there is also a good positive correlation ($r = 0.68$) for the Mn-ores of bedded-type deposits (Figure 8b).

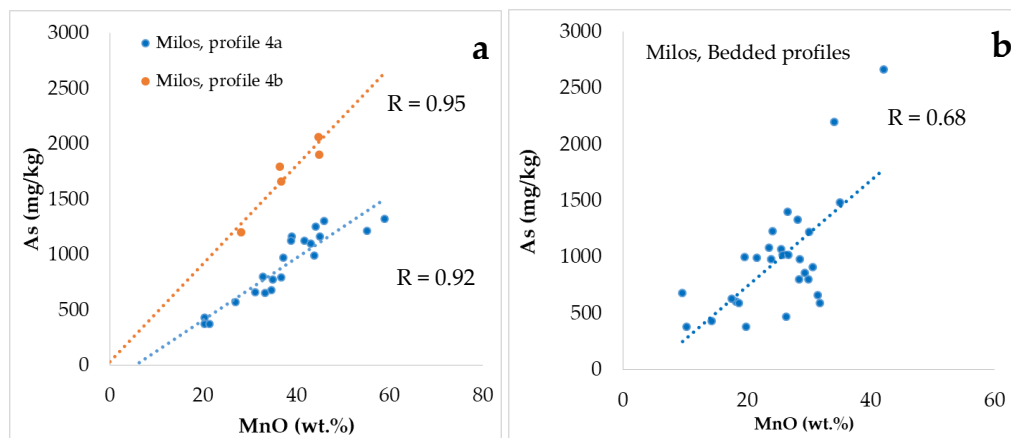


Figure 8. (a,b) Plots of As vs. MnO for Mn-Fe ores of the profile No 4a and 4b, both of “High-temperature hydrothermal Mn deposits” (Figure 5a) and “Bedded hydrothermal Mn deposits” (Figure 5b). Data from [10,11].

The compositions of almost all studied samples are plotted in the field of hydrothermal deposits of the ternary discrimination diagram [Mn-Fe-10 × (Ni + Cu + Co)], except from the Grammatiko supergene ore (Figure 9; Table 2).

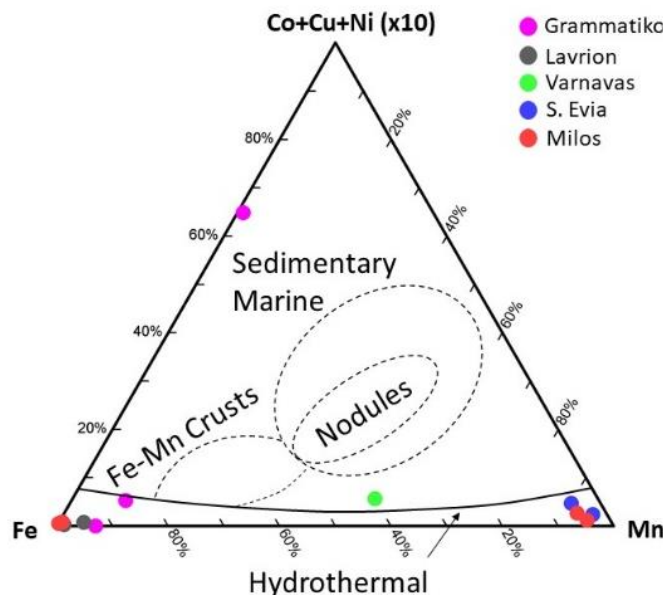


Figure 9. Ternary plot Mn-Fe-10 × (Ni + Cu + Co) discriminating marine hydrogenetic and hydrothermal Mn oxides (fields after [59–61]). Data from Table 2.

5. Discussion

5.1. Metallogenetic Signatures

Generally, manganese oxides occur in a wide range of environmental settings and exhibit a wide compositional variation in the Fe-Mn ores. This, may reflect factors affecting

the present features of each mineralization, including the composition of the ore-forming system during the precipitation of Fe and Mn, along with the incorporated minor and trace elements and post depositional changes (diagenesis and meta-diagenesis processes).

The higher Mn and Ba content is a common feature of the Mn-Fe deposits at the areas of Varnavas, S. Evia and Milos compared to the Fe-Mn deposits from Grammatiko, Lavrion (Legrena) and Hymittos (Table 1; [34]). Furthermore, a characteristic feature of the “high temperature” Mn-Fe deposits of Milos island (Vani) is their higher Ba, As, W, Cu, Pb, and Zn content compared to those of bedded Mn-deposits, forming discrete layers within volcanoclastic sandstones of the Milos island (bedded Mn) that exhibit elevated Fe, Ti, Al, K, Mg, and Ca content (Tables 1 and 2; [5,10]). Systematic patterns, on the basis of the available analytical data, are not obvious. However, plots of these data along profiles from previous publications [10] reveal a very good positive correlation ($r > 0.9$) between MnO and As content for a profile (No4) concerning a large number of samples of “high-temperature” Mn-ores, except only a few samples (Figure 5a). In addition, there is a good correlation ($r = 0.68$) for “Bedded hydrothermal Mn deposits” (Figure 5b), coupled with the variation of Fe, Ti, and Mn in the above two types of Mn mineralization that may suggest a fractionation and evolution in the ore forming system (Table 2). In addition, the Mn-Fe mineralization at Milos island is characterized by elevated W values (up to 2870 ppm W) for the Vani manganese deposit, which is considered to be a feature of High-T deposits [10]. Thus, the ore-forming system, suggesting the formation of the Milos Mn deposit during the first stage of boiling of the hydrothermal fluid resulting in the deposition of mainly pyrolusite and ramsdellite, may be followed by the precipitation of sulfides and the replacement of the primary manganese oxide minerals by cryptomelane, hollandite, coronadite, and hydrohaeterolite as well as the enrichment of minerals in K, Ba, Pb, and Zn [7,10,11]. Furthermore, the higher As content in Mn-Fe ores from the Milos and Varnavas mineralization (Table 2) may suggest a stronger oxidation capacity for As(III) in Mn deposits with a high Mn:Fe ratio and increasing pH from 6 to 7.9, while As(III) adsorption efficiency of the ores are increased with increasing Fe content. The Mn-bearing fine-grained magnetite showing 5.5 to 6.4 wt.% MnO and 1.2 to 4.9 wt.% MnO, in the Mn-Fe deposits from Varnavas and S. Evia, respectively (Table 1; [62]), is a salient mineralogical feature, too. Magnetite with significant Mn content has been described as a result of post deposition processes, during low metamorphism and multistage deformation events [63].

5.2. Bio-Mineralization

Apart from supergene processes, which may be superimposed over hydrothermal phases, present mineralogical, mineral chemistry and geochemical data (Figures 3–8; Tables 1 and 2) provide evidence for the involvement of micro-organisms during a multistage evolution of Lavrion (Legrena) Fe-Mn deposit, as well as in the Varnavas Mn-Fe deposit, similar to those from the Vani (Milos Island) (Figures 5–7; [1–10]). It has been referred that micro-organisms are widespread everywhere on and under the surface of Earth even some km depth, the submarine action of micro-organisms is known to occur some hundreds of meters below the seafloor, under survive boiling water, they are tolerate at extreme cold snow surfaces on Antarctica and extreme salt concentration, extreme radiation, acidic conditions (pH ~ 3.6) and metal concentrations (e.g., some 1000 ppm As) [13,15,64–68] and references therein. A consortium of micro-organism fossils (pointed by white and black arrows) including rods, sphere or coccus, filament-type, exhibiting a variation in their chemical composition were found in Fe-Mn deposits in Varnavas, Grammatiko, Legrena and Milos (Figures 3, 5, 6 and 8; Table 1), suggesting that bio-geochemical processes may be a driving force for bio-mineralization. It has been accepted that bio-minerals may be formed as a by-product of metabolic activity or organic matter–metal interaction, being a powerful catalyst that catalyzes redox reactions [15,69]. Negatively charged surfaces of bacteria cells offer extensive surfaces for biosorption of metals where elements with a higher positive charge are preferentially adsorbed [13,70–74]. Such Fe-Mn oxides precipitated by micro-organism mediation may play an important role in scavenging elements from the

environment of their precipitation. Recently, many authors proposed that micro-organisms are a driving force for the precipitation of manganese minerals via complicated biochemical and geo-biological processes [64–68,75]. Micro-organism-mediated Mn ore-forming systems have been widely reported in the global manganese deposits [76]. The biogenic hydrothermal Mn oxide mineralization in the Mn-ores on Milos (Vani) Island, Greece has been well established on the basis of combined petrographic micro-texture, scanning electron microscopy (SEM), transmission electron microscopy (TEM), organic (lipid) analyses and bulk and lipid specific stable C_{organic} isotope composition of matter and fluid inclusion data [13,67,75]. Those authors concluded that geothermal metalliferous fluids that vent into the shallow environments may interplay with microbial mat colonization, during pre-burial curing/diagenesis, in a mineralizing environment that favors biologically-mediated Mn^{2+} (aq) oxidation into Mn(III/IV) oxides.

5.3. Genetic Significance of Fossilized Micro-Organisms Coated by Sodium Chloride

There is still debate on whether such Mn minerals are of direct organic or inorganic origin. Laboratory studies have demonstrated that framboidal and botryoidal can occur in abiotic laboratory systems where supersaturating conditions appear to be the overriding factor controlling their formation [77]. However, the laboratory experiments were conducted at temperatures above 60 °C, which is much higher than the ambient temperature of most sedimentary environments [77] and recent studies of the internal structure of framboid within a microbial biofilm suggest that the organic matrix may play a prominent role in the nucleation of microcrystals that form framboids [9,13,20,55,56,67].

The most significant feature of fossilized bacteria in the Varnavas and Milos Mn-Fe mineralizations, is the coating by a film composed of Na and Cl in a proportion close to that of sodium chloride (NaCl) (Table 1), while bacterio-morphic oxides/hydroxides from the Legrena valley (Lavrion) contain significant amounts of Na and Cl as well (Table 1; [78]. High concentrations of salt occur in natural environments (in the Dead Sea and the Great Salt Lake) and salt-loving (halophilic) micro-organisms are known to be grown in salt solutions above seawater salinity (~3.5% salt) up to saturation ranges of approximately 35% salt in Utah [69–82]. Thus, the fossilized NaCl coated bacteria in the Varnavas and Milos may have been formed when the environment of their growth lost most of its water through evaporation and became an extremely saline water/brine. A chemoautotrophic way of life described earlier [83] has been suggested for these organisms, as no prominent coloration was found in accumulations of these cells. However, the presence of photosynthetic pigments and the possibility of a phototrophic way of life cannot be strictly excluded [84].

5.4. Implications of Micro-Organisms to the Mn Recovery

As Mn is a crucial element in many activities in the energy transition era, steel, glass, battery, and chemical industry [85,86] exploitation of low-grade Mn ores has become a challenge in dealing with the exhaustion of high-grade ore reserves and the increasing demand of Mn [19,86,87].

High grade Mn ores (>40%) are conventionally processed into manganese metal and its alloys by the pyro-metallurgical processes. However, the rapid growing demand for manganese metal attention has shifted to the low-grade manganese ores (<40%). As conventional pyro-metallurgy cannot be applied for processing those low-grade manganese ores [88], other processes are being investigated for this purpose. The reductive acid leaching process has been proposed as a cost-effective method, based on the conversion of the insoluble MnO_2 of manganese ores into soluble MnO and further to $MnSO_4$ by an acid solution without pre-calcination of manganese ores [89]. However, bioleaching has been proposed as a low-cost and environmentally friendly, alternative method for Mn metal extraction from the low grade manganese ores. Micro-organisms capable of metal recovery from those low-grade manganese ores have been well investigated and many such bacteria have been reported (e.g., [19,90,91]). Furthermore, in laboratory experiments mixed culture bioleaching has been found to be a more rapid and extensive process than that with pure

cultures [19]. Such a method could be applied to the ores investigated in this study, serving a two-tier benefit of both metal recovery and environmental beneficiation.

5.5. Environmental Implications

As presented in Tables 1 and 2, manganese iron mineralizations in ACCB contains a number of elements that, by the environmental point of view, may be assumed toxic or potentially toxic for plants, animals, and humans. Even some heavy metal ions that are essential micronutrients for plant or animal metabolism, when present in excess, can become extremely toxic [92,93]. One of the main concerns related to the potentially toxic elements present in the human environment is their predisposition to bio-accumulate. Bio-accumulation means an increase in the concentration of a chemical in a biological organism over time, compared to the chemical's concentration in the environment [94]. For example, in the Neogene basins of Attica (ACCB), the bio-accumulation factor for As ($A_{s_{\text{plant}}}/A_{s_{\text{soil}}} \times 100$) ranges from 0.02 to 9.0% [22]; the combination with the mineralogical and geochemical data may provide evidence for their contribution of detrital and chemical components from the erosion of Grammatiko and Lavrion Fe-Mn deposits and host rocks [41,42,50,51,93]. Moreover, the presence of Fe and manganese oxides increases As mobility and its availability in soil [95]. It should be noted that the content of Mn and Fe along with Pb, Zn, Cu, in soils from the neighborhood of the idle mining area of Lavrion (Attica) have been reported to range up to several thousand ppm, comprising a severe environmental thread, because of the leachability and potential bioavailability of these elements [93].

Furthermore, the Mn-Fe samples from Milos (Table 2) exhibit the highest tungsten content, while those from Varnavas present high values as well. The positive correlation between MnO and W, combined with a negative correlation between MnO and Fe_2O_3 suggests the preference of W to Mn-minerals. The geochemical properties of W are similar to those of Mo and in several minerals the substitution of W for Mo is observed. Predominate minerals contain the anionic form of the metal, $(WO_4)^{2-}$. Tungsten is potentially a very important environmental pollutant; thus, when high concentrations of tungsten are exposed in the environment, the route of dispersion, fate, and bioaccumulation through trophic levels, should be given thorough attention. Typical transformation processes for tungsten in soil include precipitation, complexation, and anion exchange. Important factors affecting the transformation of tungsten in soils and sediments include pH, ionic strength (i.e., salinity), redox potential, concentration and distribution of species, composition of the mineral matrix, organic matter, and temperature [96]. The bio-accumulation factor for tungsten ($W_{\text{plant}}/W_{\text{soil}} \times 100$) in the Neogene basins of Attica, ranges from 58 to 3100% [12,19,42]. High concentration of W in the contaminated soils generally elevated the concentration of W in wild land plants such as trees, shrubs, and grasses [97–103]. Therefore, W is more readily mobilized under alkaline conditions [101,103]. Plants growing in a mineralized zone contained up to 18 times the background W value of 2.7 mg/kg without showing toxicity symptoms [104].

Despite the fact that arsenic, lead, and tungsten content appear to be elevated in green vegetables and plants grown in the most contaminated soils of the above-mentioned basins, it is noted that there have not been regulated limits for As, Pb, W, and other possibly toxic metals for plants.

6. Conclusions

The compilation of the presented geological, mineralogical, and geochemical data with literature on Mn-Fe deposits in the Aegean Sea (ACCB) may lead us to the following conclusions:

- The presented chemical composition of ores from Attica (Grammatiko, Legrena of W. Lavrion) belongs to the Fe-Mn type of deposit, whereas those from Evia and Milos are Mn-Fe ores and contain higher Ba content;

- The studied deposits have exhibit low Cr, Co, V, Ni, Mo, and Cd values, while Ba, As, W, Cu, Pb, and Zn content are remarkably variable. The Mn-Fe deposits of Milos exhibited the highest tungsten (W) content;
- The positive trend between MnO and W coupled with the negative trend between MnO and Fe₂O₃ suggest the preference of W to Mn-minerals;
- The occurrence of abundant bacterio-morphic Fe-Mn-oxides/hydroxides is a common feature within Mn-Fe deposits in the areas of Varnavas and Milos Island and in Fe-Mn deposits in Legrena valley, which may reflect the catalytic role of micro-organisms in redox reactions that govern the formation of those Mn-Fe and Fe-Mn mineral phases;
- The presence of micro-organisms in Fe-Mn mineralization, reflecting the presence of organic matter, suggests a shallow environment for their deposition.

Author Contributions: Conceptualization, M.E.-E. and C.V.; methodology, M.E.-E. and C.V.; formal analysis, M.E.-E.; investigation, M.E.-E., E.E.K. and C.V.; resources, C.V. and M.E.-E.; data curation, C.V., E.E.K. and M.E.-E.; validation, I.M.; writing—original draft preparation, M.E.-E.; writing—review and editing, C.V., I.M. and M.E.-E.; visualization, M.E.-E. All authors have read and agreed to the published version of the manuscript.

Funding: This research received no external funding.

Data Availability Statement: All data supporting reported results have been included in the manuscript.

Acknowledgments: The National and Kapodistrian University of Athens (NKUA) is kindly thanked for funding the APC of this paper. Vasilis Skounakis, scanning electron microscopy technician, is kindly thanked for his assistance with the SEM-EDS analyses.

Conflicts of Interest: The authors declare no conflict of interest.

References

1. Reinecke, T.; Okrusch, M.; Richter, P. Geochemistry of ferromanganoan metasediments from the island of Andros, Cycladic blueschist belt, Greece. *Chem. Geol.* **1985**, *53*, 249–278. [[CrossRef](#)]
2. Dando, P.R.; Thomm, M.; Arab, H.; Brehmer, M.; Hooper, L.; Jochimsen, B.; Schlesner, H.; Stöhr, R.; Miquel, J.; Fowler, S.W. Microbiology of shallow hydrothermal sites off Palaeochori Bay, Milos (Hellenic Volcanic Arc). *Cah. Biol.* **1999**, *39*, 369–372.
3. Dando, P.R.; Aliani, S.; Arab, H.; Bianchi, C.N.; Brehmer, M.; Cocito, S.; Fowlers, S.W.; Gundersen, J.; Hooper, L.E.; Kölbh, R.; et al. Hydrothermal studies in the Aegean Sea. *Phys. Chem. Earth B. Hydrol. Oceans Atmos* **2000**, *25*, 1–8. [[CrossRef](#)]
4. Hein, J.R.; Stamatakis, G.M.; Dowling, S.J. Trace metal-rich Quaternary hydrothermal manganese oxide and barite deposit, Milos Island, Greece. *Trans. Inst. Min. Metall. Sect. B* **2000**, *109*, 67–76. [[CrossRef](#)]
5. Hein, J.R.; Schulz, M.S.; Dunham, R.E.; Stern, R.J.; Bloomer, S.H. Diffuse flow hydrothermal manganese mineralization along the active Mariana and southern Izu-Bonin arc system, western Pacific. *J. Geophys. Res.* **2008**, *113*, B08S14. [[CrossRef](#)]
6. Hein, J.R.; Mizell, K.; Koschinsky, A.; Conrad, T.A. Deep-ocean mineral deposits as a source of critical metals for high- and green-technology applications: Comparison with land-based resources. *Ore Geol. Rev.* **2013**, *51*, 1–14. [[CrossRef](#)]
7. Alfieris, D.; Voudouris, P.; Spry, P.G. Shallow submarine epithermal Pb-Zn-Cu-Au-Ag-Te mineralization on western Milos Island, Aegean Volcanic Arc, Greece: Mineralogical, geological and geochemical constraints. *Ore Geol. Rev.* **2013**, *53*, 159–180. [[CrossRef](#)]
8. Liakopoulos, A.; Glasby, G.P.; Papavassiliou, C.T.; Boulegue, J. Nature and origin of the Vani manganese deposit, Milos, Greece: An overview. *Ore Geol. Rev.* **2001**, *18*, 181–209. [[CrossRef](#)]
9. Kiliass, S.P.; Naden, J.; Cheliotis, I.; Shepherd, T.J.; Constandinidou, H.; Crossing, J.; Simos, I. Epithermal gold mineralization in the active Aegean volcanic arc: The Profitis Ilias deposit, Milos Island, Greece. *Miner. Depos.* **2001**, *36*, 32–44. [[CrossRef](#)]
10. Glasby, G.P.; Papavassiliou, C.T.; Mitsis, J.; Valsami-Jones, E.; Liakopoulos, A.; Renner, R.M. The Vani manganese deposit, Milos Island, Greece: A fossil stratabound Mn-Ba-Pb-Zn-As-Sb-W-rich hydrothermal deposit. In *Developments in Volcanology*; Fytikas, M., Vougioukalakis, G.E., Eds.; Elsevier: Amsterdam, The Netherlands, 2005; Volume 7, pp. 255–288. [[CrossRef](#)]
11. Papavassileiou, K.; Voudouris, P.; Kanellopoulos, C.; Glasby, G.; Alfieris, D.; Mitsis, I. New geochemical and mineralogical constraints on the genesis of the Vani hydrothermal manganese deposit at NW Milos Island, Greece: Comparison with the Aspro Gialoudi deposit and implications for the formation of the Milos manganese mineralization. *Ore Geol. Rev.* **2017**, *80*, 594–611. [[CrossRef](#)]
12. Sievert, S.M.; Brinkhoff, T.; Muyzer, G.; Ziebis, W.; Kuever, J. Spatial heterogeneity of bacterial populations along an environmental gradient at a shallow submarine hydrothermal vent near Milos Island (Greece). *Appl. Environ. Microbiol.* **1999**, *65*, 3834–3842. [[CrossRef](#)]
13. Chi Fru, E.; Ivarsson, M.; Kiliass, S.P.; Bengtson, S.; Belivanova, V.; Marone, F.; Fortin, D.; Broman, C.; Stampanoni, M. Fossilized iron bacteria reveal a pathway to the biological origin of banded iron formation. *Nat. Commun.* **2013**, *4*, 2050. [[CrossRef](#)]

14. Giovannelli, D.; d' Errico, G.; Manini, E.; Yakimov, M.; Vetriani, C. Diversity and phylogenetic analyses of bacteria from a shallow-water hydrothermal vent in Milos island (Greece). *Front. Microbiol.* **2013**, *4*, 184. [[CrossRef](#)]
15. Ehrlich, L.E. *Geomicrobiology*, 4th ed.; Marcel Dekker: New York, NY, USA, 2002.
16. Jackson, D.D. The precipitation of iron, manganese, and aluminum by bacterial action. *J. Soc. Chem. Ind.* **1901**, *21*, 681–684.
17. Cahyani, V.R.; Murase, J.; Ishibashi, E.; Asakawa, S.; Kimura, M. Phylogenetic positions of Mn²⁺-oxidizing bacteria and fungi isolated from Mn nodules in rice field subsoils. *Biol. Fert. Soils* **2009**, *45*, 337–346. [[CrossRef](#)]
18. Nealsen, K.H. The manganese oxidizing bacteria. In *The Prokaryotes, Proteobacteria: Alpha and Beta Subclasses*, 3rd ed.; Dworkin, M., Falkow, S., Rosenberg, E., Schleifer, E., Stackebrandt, K.H., Eds.; Springer: New York, NY, USA, 2006; Volume 5, pp. 222–231. [[CrossRef](#)]
19. Ghosh, S.; Mohanty, S.; Nayak, S.; Sukla, L.B.; Das, A.P. Molecular identification of indigenous manganese solubilising bacterial biodiversity from manganese mining deposits. *J. Basic Microbiol.* **2016**, *56*, 254–262. [[CrossRef](#)]
20. Chi Fru, E.; Kiliyas, S.; Ivarsson, M.; Rattray, J.E.; Gkika, K.; McDonald, I.; He, Q.; Broman, C. Sedimentary mechanisms of a modern banded iron formation on Milos Island, Greece. *Solid Earth* **2018**, *9*, 573–598. [[CrossRef](#)]
21. Kampouroglou, E.E. Investigation of Contamination at the Carbonic Basin in Varnavas, Attica from Arsenic and Heavy Metals and Their Source of Origin. Master's Thesis, National University of Athens, Athens, Greece, 2011. (In Greek)
22. Kampouroglou, E.; Economou-Eliopoulos, M. Assessment of arsenic and associated metals in the soil-plant-water system in Neogene basins of Attica, Greece. *Catena* **2017**, *150*, 206–222. [[CrossRef](#)]
23. Bonneau, M. Correlation of the Hellenic Nappes in the south-east Aegean and their tectonic reconstruction. In *The Geological Evolution of the Eastern Mediterranean*; Dixon, J.E., Robertson, A.H.F., Eds.; Geological Society: London, UK, 1984; Volume 17, pp. 517–527. [[CrossRef](#)]
24. Dürr, S.; Altherr, R.; Keller, J.; Okrusch, M.; Seidel, E. The median Aegean crystalline belt: Stratigraphy, structure, metamorphism, magmatism. In *Alps, Apennines, Hellenides*; Closs, H., Roeder, D.H., Schmidt, K., Eds.; IUGS Report; Schweizerbart: Stuttgart, Germany, 1978; Volume 38, pp. 455–477.
25. Altherr, R.; Kreuzer, H.; Wendt, I.; Lenz, H.; Wagner, G.A.; Keller, J.; Harre, W.; Höhdorf, A.A. Late Oligocene/Early Miocene high temperature belt in the Attic-Cycladic belt in the Attic-Cycladic crystalline complex (SE Pelagonian, Greece). *Geol. Jahrb.* **1982**, *23*, 97–164.
26. Okrusch, M.; Bröcker, M. Eclogite facies rocks in the Cycladic Blueschist Belt, Greece: A review. *Eur. J. Mineral.* **1990**, *2*, 451–478. [[CrossRef](#)]
27. Jolivet, L.; Menant, A.; Sternai, P.; Rabillard, A.; Arbaret, L.; Augier, R.; Laurent, V.; Beaudoin, A.; Grasemann, B.; Huet, B.; et al. The geological signature of a slab tear below the Aegean. *Tectonophysics* **2015**, *659*, 166–182. [[CrossRef](#)]
28. Bröcker, M.; Franz, L. The base of the Cycladic Blueschist Unit on Tinos Island (Greece) re-visited: Field relationships, phengite chemistry and Rb–Sr geochronology. *Neues Jahrb. Mineral. Abh.* **2005**, *181*, 81–93. [[CrossRef](#)]
29. Bröcker, M.; Franz, L. Dating metamorphism and tectonic juxtaposition on Andros Island (Cyclades, Greece): Results of a Rb–Sr study. *Geol. Mag.* **2006**, *143*, 609–620. [[CrossRef](#)]
30. Stouraiti, C.; Pantziris, I.; Vasilatos, C.; Kanellopoulos, C.; Mitropoulos, P.; Pomonis, P.; Moritz, R.; Chiaradia, M. Ophiolitic Remnants from the Upper and Intermediate Structural Unit of the Attic-Cycladic Crystalline Belt (Aegean, Greece): Fingerprinting Geochemical Affinities of Magmatic Precursors. *Geosciences* **2017**, *7*, 14. [[CrossRef](#)]
31. Tomaschek, F.; Kennedy, A.K.; Villa, I.M.; Lagos, M.; Ballhaus, C. Zircons from Syros, Cyclades, Greece-Recrystallization and mobilization of zircon during high pressure metamorphism. *J. Petrol.* **2003**, *44*, 1977–2002. [[CrossRef](#)]
32. Katzir, Y.; Matthews, A.; Garfunkel, Z.; Evans, B.W. Origin, HP/LT metamorphism and cooling of ophiolitic mélanges in southern Evia (NW Cyclades) Greece. *J. Metamorph. Geol.* **2000**, *18*, 699–718. [[CrossRef](#)]
33. Baziotis, I.; Mposkos, E. Origin of metabasites from upper tectonic unit of the Lavrion area (SE Attica, Greece): Geochemical implications for dual origin with distinct provenance of blueschist and greenschist's protoliths. *Lithos* **2011**, *126*, 161–173. [[CrossRef](#)]
34. Stouraiti, C.; Soukis, K.; Voudouris, P.; Mavrogonatos, C.; Lozios, S.; Lekkas, S.; Beard, A.; Strauss, H.; Palles, D.; Baziotis, I.; et al. Silver-rich sulfide mineralization in the northwestern termination of the Western Cycladic Detachment System, at Agios Ioannis Kynigos, Hymittos Mt. (Attica, Greece): A mineralogical, geochemical and stable isotope study. *Ore Geol. Rev.* **2019**, *111*, 1–16. [[CrossRef](#)]
35. Diamantopoulos, A. Non-coaxial stretching deformation dominating the Upper Structural Plate of the metamorphic core complex of Attica (Internal Hellenides, Central Greece). In Proceedings of the XVIIIth Congress of the Carpathian-Balkan Geological Association, Belgrade, Serbia, 3–6 September 2006; pp. 101–105.
36. Ioakim, C.; Rondoyanni, T.; Mettos, A. The Miocene basins of Greece (Eastern Mediterranean) from a paleoclimatic perspective. *Rev. Paleobiol.* **2005**, *24*, 735–748.
37. Lozios, S. Tectonic analysis of metamorphic formations of Northeastern Attica. Ph.D. Thesis, National and Kapodistrian University of Athens (NKUA), Athens, Greece, 1993. (In Greek)
38. Papanikolaou, D.; Royden, L.H. Disruption of the Hellenic arc: Late Miocene extensional detachment faults and steep Pliocene–Quaternary normal faults—or what happened at Corinth? *Tectonics* **2007**, *26*, TC5003. [[CrossRef](#)]
39. Papanikolaou, D.; Papanikolaou, I. Geological, geomorphological and tectonic structure of the NE Attica and seismic hazard implications for the northern edge of the Athens plain. *Bull. Geol. Soc. Greece* **2007**, *40*, 425–438. [[CrossRef](#)]

40. Skarpelis, N. Geodynamics and evolution of the Miocene mineralization in the Cycladic-Pelagonian Belt, Hellenides. *Bull. Geol. Soc. Greece* **2002**, *34*, 2191–2209. [[CrossRef](#)]
41. Skarpelis, N. The Lavrion deposit (SE Attica, Greece): Geology, mineralogy and minor elements chemistry. *Neu Jb. Mineral. Abh.* **2007**, *183*, 227–249. [[CrossRef](#)]
42. Voudouris, P.; Melfos, V.; Spry, P.; Bonsall, T.; Tarkian, M.; Economou-Eliopoulos, M. Mineralogical and fluid inclusion constraints on the evolution of the Plaka intrusion-related ore system, Lavrion, Greece. *Miner. Petrol.* **2008**, *93*, 79–110. [[CrossRef](#)]
43. Bonsall, T.A.; Spry, P.G.; Voudouris, P.; Tombros, S.; Seymour, K.; Melfos, V. The Geochemistry of Carbonate-Replacement Pb-Zn-Ag Mineralization in the Lavrion District, Attica, Greece: Fluid Inclusion, Stable Isotope, and Rare Earth Element Studies. *Econ. Geol.* **2011**, *106*, 619–651. [[CrossRef](#)]
44. Berger, A.; Schneider, D.A.; Grasemann, B.; Stockli, D. Footwall mineralization during Late Miocene extension along the West Cycladic Detachment System, Lavrion, Greece. *Terra Nova* **2013**, *25*, 181–191. [[CrossRef](#)]
45. Spry, P.; Mathur, R.; Bonsall, T.; Voudouris, P.; Melfos, V. Re-Os isotope evidence for mixed source components in carbonate-replacement Pb-Zn-Ag deposits in the Lavrion district, Attica, Greece. *Miner. Pet.* **2014**, *108*, 503–513. [[CrossRef](#)]
46. Ducoux, M.; Branquet, Y.; Jolivet, L.; Arbaret, L.; Grasemann, B.; Rabillard, A.; Gumiaux, C.; Drufin, S. Synkinematic skarns and fluid drainage along detachments: The West Cycladic Detachment System on Serifos Island (Cyclades, Greece) and its related mineralization. *Tectonophysics* **2017**, *695*, 1–26. [[CrossRef](#)]
47. Papanikolaou, D.; Lekkas, E.; Syskakis, D. Tectonic analysis of the geothermal field of Milos Island. *Bull. Geol. Soc. Greece* **1990**, *24*, 27–46.
48. Bekker, A.; Slack, F.J.; Planavsky, N.; Krapež, B.; Hofmann, A.; Konhauser, O.K.; Rouxel, J.O. Iron Formation: The Sedimentary Product of a Complex Interplay among Mantle, Tectonic, Oceanic, and Biospheric Processes. *Econ Geol* **2010**, *105*, 467–508. [[CrossRef](#)]
49. Marinos, G.P.; Petrascheck, W.E. Laurium. In *Geological and Geophysical Research*; Institute for Geology and Subsurface Research: Athens, Greece, 1956; Volume 4.
50. Skarpelis, N.; Argyraki, A. Geology and origin of supergene ore at the Lavrion Pb-Ag-Zn deposit, Attica, Greece. *Resour. Geol.* **2008**, *59*, 1–14. [[CrossRef](#)]
51. Kampouroglou, E.; Economou-Eliopoulos, M. Assessment of the environmental impact by As and heavy metals in lacustrine travertine limestone and soil in Attica, Greece: Mapping of potentially contaminated sites. *Catena* **2016**, *139*, 137–166. [[CrossRef](#)]
52. Plimer, I. *Milos Geologic History*; Koan Publishing House: Athens, Greece, 2000.
53. Skarpelis, N.; Koutles, T. Geology of epithermal mineralization of the NW part of Milos island, Greece. In Proceedings of the 5th International Symposium on Eastern Mediterranean Geology, Thessaloniki, Greece, 14–20 April 2004.
54. Stewart, A.L.; McPhie, J. Facies architecture and Late Pliocene—Pleistocene evolution of a felsic volcanic island, Milos, Greece. *Bull. Volcanol.* **2006**, *68*, 703–726. [[CrossRef](#)]
55. Kiliass, S.P. Microbial-Mat Related Structures in the Quaternary Cape Vani Manganese Oxide(-Barite) Deposit, NW Milos Island-Greece. In *Microbial Mats in Siliciclastic Depositional Systems Through Time*; Noffke, N., Chafetz, H., Eds.; SEPM (Society for Sedimentary Geology) Special Publication: Broken Arrow, OK, USA, 2012; Volume 101, pp. 97–110.
56. Chi Fru, E.; Ivarsson, M.; Kiliass, S.P.; Frings, P.J.; Hemmingsson, C.; Broman, C.; Bengtson, S.; Chatzitheodoridis, E. Biogenicity of an Early Quaternary iron formation, Milos Island, Greece. *Geobiology* **2015**, *13*, 225–244. [[CrossRef](#)]
57. Galanopoulos, E.; Charmatzis, C. Mineralogical Study of Metamorphosed Manganiferous Sediments from the Varnavas Area in Attica, and Their Relation to Similar Horizons in South Evia and Andros. Island. Greece. Bachelor's Thesis, National and Kapodistrian University of Athens (NKUA), Athens, Greece, 2007.
58. Wu, S.F.; You, C.F.; Lin, Y.P.; Valsami-Jones, E.; Baltatzis, E. New boron isotopic evidence for sedimentary and magmatic fluid influence in the shallow hydrothermal vent system of Milos Island (Aegean Sea, Greece). *J. Volcanol. Geoth. Res.* **2016**, *310*, 58–71. [[CrossRef](#)]
59. Bonatti, E.; Kraemer, T.; Rydell, H. Classification and genesis of submarine iron manganese deposits. In *Ferromanganese Deposits on the Ocean Floor*; Horn, D., Ed.; National Science Foundation: Washington, DC, USA, 1972; pp. 149–166.
60. Corliss, J.B.; Dymond, J. Nazca plate metalliferous sediments: I. Elemental distribution patterns in surface samples. *Trans. Am. Geophys. Union* **1975**, *56*, 445.
61. Toth, J.R. Deposition of submarine crusts rich in manganese and iron. *Geol. Soc. Am. Bull.* **1980**, *91*, 44–55. [[CrossRef](#)]
62. Ghikas, J. Manganese Rich Rocks of Southern Evia. Bachelor's Thesis. National and Kapodistrian University of Athens (NKUA), Athens, Greece, 2014; p. 33.
63. Scheffer, C.; Tarantola, A.; Vanderhaeghe, O.; Voudouris, P.; Rigaudier, T.; Photiades, A.; Morin, D.; Alloucherie, A. The Lavrion Pb-Zn-Fe-Cu-Ag detachment-related district (Attica, Greece): Structural control on hydrothermal flow and element transfer-deposition. *Tectonophysics* **2017**, *717*, 607–627. [[CrossRef](#)]
64. Hansel, M.C.; Learman, R.D. Geomicrobiology of Manganese. In *Ehrlich's Geomicrobiology*, 6th ed.; Ehrlich, L.H., Dianne, K., Newman, D.K., Kappler, A., Eds.; CRC Press Taylor & Francis Group: Boca Raton FL, USA, 2015; pp. 401–452.
65. Fischer, W.W.; Hemp, J.; Johnson, J.E. Manganese and the Evolution of Photosynthesis. *Orig. Life Evol. Biosph.* **2015**, *45*, 351–357. [[CrossRef](#)]
66. Polgári, M.; Gyollai, I.; Fintor, K.; Horváth, H.; Pál-Molnár, E.; Biondi, J.C. Microbially Mediated Ore-Forming Processes and Cell Mineralization. *Front. Microbiol.* **2019**, *10*, 2731. [[CrossRef](#)]

67. Kiliyas, S.P.; Ivarsson, M.; Chi Fru, E.C.; Rattray, J.E.; Gustafsson, H.; Naden, J.; Detsi, K. Precipitation of Mn oxides in quaternary microbially induced sedimentary structures (MISS), Cape Vani paleo-hydrothermal vent field, Milos, Greece. *Minerals* **2020**, *10*, 536. [[CrossRef](#)]
68. Gracheva, M.; Homonnay, Z.; Kovács, K.; Kende Attila Béres, K.A.; Biondi, J.C.; Yu, W.; Kovács Kis, V.; Gyollai, I.; Polgári, M. Mössbauer characterization of microbially mediated iron and manganese ores of variable geological ages. *Ore Geol. Rev.* **2021**, *134*, 104124. [[CrossRef](#)]
69. Lowenstam, A.H.; Weiner, S. *On Biomineralization*; Oxford University Press: New York, NY, USA, 1989.
70. Pósfai, M.; Buseck, P.R.; Bazylinski, D.A.; Frankel, R.B. Iron sulfides from magnetotactic bacteria: Structure, compositions, and phase transitions. *Am. Min.* **1998**, *83*, 1469–1481. [[CrossRef](#)]
71. Haferburg, G.; Kothe, E. Microbes and metals: Interactions in the environment. *J. Basic Microbiol.* **2007**, *47*, 453–467. [[CrossRef](#)]
72. Navrotsky, A.; Mazeina, L.; Majzslan, J. Size driven structural and thermodynamic complexity in iron oxides. *Science* **2008**, *319*, 1635–1638. [[CrossRef](#)]
73. Laskou, M.; Economou-Eliopoulos, M. The role of microorganisms on the mineralogical and geochemical characteristics of the Parnassos-Ghiona bauxite deposits, Greece. *J. Geochem. Explor.* **2007**, *93*, 67–77. [[CrossRef](#)]
74. Laskou, M.; Economou-Eliopoulos, M. Bio-mineralization and potential biogeochemical processes in bauxite deposits: Genetic and ore quality significance. *Miner. Petrol.* **2013**, *107*, 471–486. [[CrossRef](#)]
75. Ivarsson, M.; Kiliyas, S.P.; Broman, C.; Neubeck, A.; Drake, H.; Chi Fru, E.; Bengtson, S.; Naden, J.; Detsi, K.; Whitehouse, M.J. Exceptional preservation of fungi as H₂-bearing fluid inclusions in an early Quaternary paleohydrothermal system at Cape Vani, Milos, Greece. *Minerals* **2019**, *9*, 749. [[CrossRef](#)]
76. Polgári, M.; Hein, J.R.; Vigh, T.; Szabó-Drubina, M.; Fórizs, I.; Bíró, L.; Müller, A.; Tóth, A.L. Microbial processes and the origin of the Úrkút manganese deposit, Hungary. *Ore Geol. Rev.* **2012**, *47*, 87–109. [[CrossRef](#)]
77. Ohfuji, H.; Rickard, D. Experimental syntheses of framboids. A review. *Earth Sci. Rev.* **2005**, *71*, 147–170. [[CrossRef](#)]
78. Vasilatos, C.; Economou-Eliopoulos, M. Fossilized Bacteria in Fe-Mn-Mineralization: Evidence from the Legrena Valley, W. Lavrion Mine (Greece). *Minerals* **2018**, *8*, 107. [[CrossRef](#)]
79. Denner, E.B.M.; McGenity, T.J.; Busse, H.J.; Grant, W.D.; Wanner, G.; Stan-Lotter, H. *Halococcus isalifodinae* sp. nov., an archaeal isolate from an Austrian salt mine. *Int. J. Syst. Bacteriol.* **1994**, *44*, 774–780. [[CrossRef](#)]
80. Gruber, C.; Legat, A.; Pfaffenhuemer, M.; Radax, C.; Weidler, G.; Busse, H.J.; Stan-Lotter, H. *Halobacterium noricense* sp. nov., an archaeal isolate from a bore core of an alpine Permian salt deposit, classification of *Halobacterium* sp. NRC-1 as a strain of *H. salinarum* and emended description of *H. salinarum*. *Extremophiles* **2004**, *8*, 431–439. [[CrossRef](#)]
81. Stan-Lotter, H.; McGenity, T.J.; Legat, A.; Denner, E.B.M.; Glaser, K.; Stetter, K.O.; Wanner, G. Very similar strains of *Halococcus salifodinae* are found in geographically separated Permo-Triassic salt deposits. *Microbiology* **1999**, *145*, 3565–3574. [[CrossRef](#)]
82. Stan-Lotter, H.; Pfaffenhuemer, M.; Legat, A.; Busse, H.J.; Radax, C.; Gruber, C. *Halococcus dombrowskii* sp. nov., an archaeal isolate from a Permian alpine salt deposit. *Int. J. Syst. Evol. Microbiol.* **2002**, *52*, 1807–1814.
83. Oren, A.; Köhl, M.; Karsten, U. An endoevaporitic microbial mat within a gypsum crust: Zonation of phototrophs, photopigments and light penetration. *Mar. Ecol. Prog. Ser.* **1995**, *128*, 151–159. [[CrossRef](#)]
84. Caffari, S.; Tibiletti, T.; Jennings, R.C.; Santabarbara, S. A comparison between plant Photosystem I and Photosystem II architecture and functioning. *Curr. Protein Pept. Sci.* **2014**, *15*, 296–331. [[CrossRef](#)]
85. Das, A.P.; Ghosh, S.; Mohanty, S.; Sukla, L.B. Advances in Manganese Pollution and Its Bioremediation. In *Environmental Microbial Biotechnology; Soil Biology*; Sukla, L., Pradhan, N., Panda, S., Mishra, B., Eds.; Springer: Cham, Switzerland, 2015; Volume 45. [[CrossRef](#)]
86. Su, H.; Liu, H.; Wang, F.; Lü, X.; Wen, Y. Kinetics of reductive leaching of low grade pyrolusite with molasses alcohol waste water in H₂SO₄. *Chin. J. Chem. Eng.* **2010**, *18*, 730–735. [[CrossRef](#)]
87. Srichandan, H.; Kim, D.J.; Gahan, C.S.; Akcil, A. Microbial extraction metal values from spent catalyst: Mini review. Chapter 11; In *Advances in Biotechnology*; Thatoi, H.N., Ed.; Indian Publisher: New Delhi, India, 2013; pp. 225–239.
88. Zhang, W.; Cheng, C. Manganese metallurgy review. Part I: Leaching of ores/secondary materials and recovery of electrolytic/chemical manganese dioxide. *Hydrometallurgy* **2007**, *89*, 137–159. [[CrossRef](#)]
89. Xiong, S.; Li, X.; Liu, P.; Hao, S.; Hao, F.; Yin, Z.; Liu, J. Recovery of manganese from low-grade pyrolusite ore by reductively acid leaching process using lignin as a low cost reductant. *Miner. Eng.* **2018**, *125*, 126–132. [[CrossRef](#)]
90. Das, A.P.; Sukla, L.B.; Pradhan, N.; Nayak, S. Manganese biomining: A review. *Bioresour Technol* **2011**, *102*, 7381–7387. [[CrossRef](#)]
91. Panda, S.; Biswal, A.; Mishra, S.; Panda, P.K.; Pradhan, N.; Mohapatra, U.; Sukla, L.B.; Mishra, B.K.; Akcil, A. Reductive dissolution by waste newspaper for enhanced meso-acidophilic bioleaching of copper from low grade chalcopyrite: A new concept of biohydrometallurgy. *Hydrometallurgy* **2015**, *153*, 98–105. [[CrossRef](#)]
92. Begum, A. Concurrent removal and accumulation of Fe²⁺, Cd²⁺ and Cu²⁺ from waste water using aquatic macrophytes. *Der. Pharma Chem.* **2009**, *1*, 219–224.
93. Giannatou, S.; Vasilatos, C.; Mitsis, I.; Koukouzas, N.; Itskos, G.; Stamatakis, M.G. Reduction of toxic element mobility in acid mine soils by zeolitic amendments. *Bull. Geol. Soc. Greece* **2016**, *50*, 2127–2136. [[CrossRef](#)]
94. Mohan, K.; Syed Shafi, S. Removal of cadmium from the aqueous solution using chitin/polyethylene glycol binary blend. *Der. Pharm. Lett.* **2013**, *5*, 62–69.

95. Zavala, Y.J.; Duxbury, J.M. Arsenic in rice: Estimating normal levels of total arsenic in rice grain. *Environ. Sci. Technol.* **2008**, *42*, 3856–3860. [[CrossRef](#)]
96. Lin, C.Y.; Negev, I.; Eshel, G.; Banin, A. In Situ Accumulation of Copper, Chromium, Nickel, and Zinc in Soils Used for Long-term Waste Water Reclamation. *J. Environ. Qual.* **2008**, *37*, 1477–1487. [[CrossRef](#)]
97. Quin, B.F.; Brooks, R.R. The tungsten contents of some plants from a mineralized area in New Zealand. *N. Z. J. Sci.* **1972**, *15*, 308–312.
98. Quin, B.F.; Brooks, R.R. Tungsten concentrations in plants and soils as a means of detecting scheelite-bearing ore-bodies in New Zealand. *Plant Soil* **1974**, *41*, 177–188. [[CrossRef](#)]
99. Pyatt, F.B.; Pyatt, A.J. The bioaccumulation of tungsten and copper by organisms inhabiting metalliferous areas in North Queensland, Australia: An evaluation of potential health implications. *J. Environ. Health Res.* **2004**, *3*, 13–18.
100. Wilson, B.; Pyatt, F.B. Bioavailability of tungsten in the vicinity of an abandoned mine in the English Lake District and some potential health implications. *Sci. Total Environ.* **2006**, *370*, 401–408. [[CrossRef](#)] [[PubMed](#)]
101. Wilson, B.; Pyatt, F.B. Persistence and bioaccumulation of tungsten and associated heavy metals under different climatic conditions. *Land Contam. Reclam.* **2009**, *17*, 93–100. [[CrossRef](#)]
102. Wilson, B.; Pyatt, F.B. Bioavailability of tungsten and associated metals in calcareous soils in the vicinity of an ancient metalliferous mine in the Corbieres area, Southwestern France. *J. Toxicol. Environ. Health* **2009**, *A72*, 807–816. [[CrossRef](#)] [[PubMed](#)]
103. Jiang, F.; Heilmeier, H.; Hartung, W. Abscisic acid relations of plants grown on tungsten enriched substrates. *Plant Soil* **2007**, *301*, 37–49. [[CrossRef](#)]
104. Bednar, A.J.; Boyd, R.E.; Jones, W.T.; McGrath, C.J.; Johnson, D.R.; Chappell, M.A.; Ringelberg, D.B. Investigations of tungsten mobility in soil using column tests. *Chemosphere* **2009**, *75*, 1049–1056. [[CrossRef](#)]